doi:10.1006/jmbi.2001.5304 available online at http://www.idealibrary.com on IDEAL® J. Mol. Biol. (2002) 316, 51–64

JMB

Biochemical and Crystallographic Studies of the Met144Ala, Asp92Asn and His254Phe Mutants of the Nitrite Reductase from *Alcaligenes xylosoxidans* Provide Insight into the Enzyme Mechanism

Mark J. Ellis[1,2], Miguel Prudêncio[3], Fraser E. Dodd[2], Richard W. Strange[2] Gary Sawers[3], Robert R. Eady[4] and S. Samar Hasnain[1,2]*

[1]*Faculty of Applied Science, De Montfort University, Leicester LE1 9BH, UK*

[2]*Molecular Biophysics Group CLRC Daresbury Laboratory Warrington, WA4 4AD, UK*

[3]*Molecular Microbiology Department John Innes Centre Norwich, NR4 7HU, UK*

[4]*Biological Chemistry Department, John Innes Centre Norwich, NR4 7HU, UK*

Dissimilatory nitrite reductase catalyses the reduction of nitrite (NO_2^-) to nitric oxide (NO). Copper-containing nitrite reductases contain both type 1 and type 2 Cu sites. Electron transfer from redox partners is presumed to be mediated *via* the type 1 Cu site and used at the catalytic type 2 Cu centre along with the substrate nitrite. At the type 2 Cu site, Asp92 has been identified as a key residue in substrate utilisation, since it hydrogen bonds to the water molecule at the nitrite binding site. We have also suggested that protons enter the catalytic site *via* Asp92, through a water network that is mediated by His254. The role of these residues has been investigated in the blue copper nitrite reductase from *Alcaligenes xylosoxidans* (NCIMB 11015) by a combination of point mutation, enzymatic activity measurement and structure determination.

In addition, it has been suggested that the enzyme operates *via* an ordered mechanism where an electron is transferred to the type 2 Cu site largely when the second substrate nitrite is bound and that this is controlled *via* the lowering of the redox potential of the type 2 site when it is loaded with nitrite. Thus, a small perturbation of the type 1 Cu site should result in a significant effect on the activity of the enzyme. For this reason a mutation of Met144, which is the weakest ligand of the type 1 Cu, is investigated. The structures of H254F, D92N and M144A have been determined to 1.85 Å, 1.9 Å and 2.2 Å resolution, respectively. The D92N and H254F mutants have negligible or no activity, while the M144A mutant has ~30% activity of the native enzyme. Structural and spectroscopic data show that the loss of activity in H254F is due to the catalytic site being occupied by Zn while the loss/reduction of activity in D92N/M144A are due to structural reasons. The D92N mutation results in the loss of the Asp92 hydrogen bond to the Cu-ligated water. Therefore, the ligand is no longer able to perform proton abstraction. Even though the loss of activity in H254F is due to lack of catalytic Cu, the mutation does cause the disruption of the water network, confirming its key role in proton channel. The structure of the H254F mutant is the first case where full occupancy Zn at the type 2 Cu site is observed, but despite the previously noted similarity of this site to the carbonic anhydrase catalytic site, no carbonic anhydrase activity is observed. The H254F and D92N mutant structures provide, for the first time, observation of surface Zn sites which may act as a Zn sink and prevent binding of Zn at the catalytic Cu site in the native enzyme.

Present address: M. Prudêncio, Leiden Institute of Chemistry, Gorlaeus Laboratories, Leiden University, Einsteinweg 55/P.O. Box 9502 2300RA, Leiden, The Netherlands.

Abbreviations used: NiR, nitrite reductase; EPR, electron paramagnetic resonance; SOD, superoxide dismutase.

E-mail address of the corresponding author: S.Hasnain@dl.ac.uk

0022-2836/02/010051–14 $35.00/0

*Corresponding author

Keywords: nitrite reductase; cupredoxin; enzyme mechanism; metalloproteins; *Alcaligenes xylosoxidans*

Introduction

Nitrogen is introduced into the biosphere by biological and chemical fixation of dinitrogen (N_2) and removed by the process of denitrification. Denitrification is an anaerobic respiratory pathway by which some bacteria carry out the sequential reduction of nitrate *via* nitrite, NO and N_2O as intermediates to dinitrogen. In addition to the importance of this process in bioenergetics, further impetus for the study of the denitrification process is provided by its environmental impact. This ranges from the production of NO as a pollutant and N_2O as a potent greenhouse gas, following CO_2 and CH_4 in its contribution to global warming. Dissimilatory nitrite reductase (NiR) is a key enzyme in denitrification since it catalyses the reduction of nitrite to NO, the first committed step of denitrification. Denitrification results in the significant loss of fixed nitrogen from the terrestrial environment.[1,2]

Two types of NiRs are found in the denitrifying bacteria, the cytochrome cd_1 and Cu NiRs (CuNiR); the latter is more widespread, being found in bacteria occupying a greater variety of habitats. CuNiRs have been isolated and characterised from a number of bacterial sources, including *Alcaligenes faecalis S-6* (*Af*NiR),[3] *Alcaligenes xylosoxidans* (*Ax*NiR),[4,5] *Achromobacter cycloclastes* (*Ac*NiR)[6] and *Pseudomonas aureofaciens* (*Pa*NiR).[7] CuNiRs are classified as either blue (*Ax*NiR and *Pa*NiR) or green (*Af*NiR and *Ac*NiR) depending on their visible absorption spectra.

A number of suggestions have been offered in order to explain why some NiRs are blue (*Ax*NiR) and others are green (*Af*NiR), though it is widely accepted that the conformation of Met144 is responsible. One suggestion is that residue 171, which is a Thr in *Ax*NiR but Tyr in *Af*NiR, may regulate the colour of the protein.[8] This is based on the effect of the side-chain volume and hydrogen bonding to the β-sheet containing the T1Cu ligand. However, the ring oxygen of the Tyr is poorly positioned to produce this hydrogen bond. A more favourable hydrogen bond, between the two β-sandwiches with Greek key motif, is evident at this point. An alternative explanation is that several hydrogen bonds near the Cu ligating Met of *Af*NiR are not present in *Ax*NiR. These are from Gln181 $O^{\varepsilon 1}$ to Asn151 $N^{\delta 2}$, Val146 O to Asn151 $N^{\delta 2}$, and Gly149 O to Asn151 N. These hydrogen bonds may cause a slight change in the position of the Met C^{α} and hence result in a change in the Met side-chain from the chair to the boat conformation. The only bond present in *Ax*NiR is between Gly143 O and Ser145 N (the *Af*NiR Gly149 and Asn151 equivalents).

The trimeric structures of several of the CuNiRs have now been established by X-ray crystallography; *Ac*NiR,[9] *Af*NiR[10] and *Ax*NiR;[11] and solution X-ray scattering; *Ax*NiR,[12] *Pa*NiR and *Af*NiR.[13] The crystal structures of the three CuNiRs show that they are similar, with each monomer or subunit consisting of two domains with the characteristic β-sandwich and Greek key motif, similar to those found in cupredoxins. Each subunit contains a buried type 1 Cu (T1Cu) site and a type 2 Cu (T2Cu) site located at the subunit interface, with Cu ligands provided by two subunits. The T1Cu site accepts electrons from an azurin/pseudoazurin, which transfer to the T2Cu centre where nitrite reduction occurs. The proposed mechanism for CuNiRs is that nitrite binds to the T2Cu replacing a water molecule. The T2Cu is then reduced *via* an electron transfer from the T1Cu, allowing reduction of nitrite to take place.[14]

Cloning and sequencing of the *Ax*NiR gene has allowed the recombinant protein to be synthesised.[15] Site-directed mutagenesis has been used to produce recombinant proteins incorporating single point mutations to investigate the role of the Cu ligands in the nitrite reduction process.

The T1Cu site of NiR is similar to that found in other T1Cu-containing proteins, namely, a distorted trigonal planar geometry formed from the three strong planar ligands; His139 $N^{\delta 1}$, His89 $N^{\delta 1}$ and Cys130 S^{γ}. A weaker fourth axial ligand, Met144 S^{δ}, completes the Cu coordination. The role of the axial ligand has been extensively discussed in terms of regulation of the redox potential of cupredoxins.[16–18] This has been supported by work conducted on azurins.[19] The M144A mutation in *Ax*NiR should afford us a better understanding of its role. The M148E (the *Ax*NiR M144 equivalent) mutation in *Af*NiR results in the replacement of the T1Cu with Zn.[20]

It has been proposed that protons are delivered to the T2Cu site *via* a highly ordered hydrogen-bonded water network.[11] This network extends along the monomer-monomer interface, from the surface of the protein to the T2Cu. There would appear to be two key protein residues in this network. His254 resides halfway along a hydrogen-bound water network. It extends into the channel and may provide gating of proton flow. The second residue is Asp92, which is situated at the T2Cu site. It hydrogen bonds the Cu co-ordinating water (W503) and a second water at the end of the proton channel (W600).

Point mutations of Asp92 have been carried out on a number of species of NiR[21–23] resulting in negligible activity of the enzyme in comparison with the native protein. Crystallographic studies of this mutation in *Af*NiR have shown that the Asn is

rotated by some 40° and is no longer in a favourable position to allow hydrogen bonding to the Cu-ligating water.[21]The crystallographic structure of D92N of *Ax*NiR reported here shows that the Cu-ligating water is indeed no longer hydrogen bonded to residue 92 but has moved around the Cu centre. However, unlike the mutation of *Af*NiR there is no rotation of the Asn side-chain.

Here we also report the results of the mutation H254F which affects the hydrogen bonded water network. The crystal structure of H254F confirms this residue's key role in the proton channel.

Results and Discussion

Optical spectroscopy

M144A shows only a single absorbance band in the 600 nm region ($\varepsilon_{593} = 4.667\ mM^{-1}\ cm^{-1}$), which is indicative of a simple blue-copper protein. H254F exhibits a strong absorbance peak at 593 nm ($\varepsilon_{593} = 5.71\ mM^{-1}cm^{-1}$) and a weaker absorbance at 470 nm ($\varepsilon_{470} = 0.75\ mM^{-1}\ cm^{-1}$) and while the 593 nm peak is similar in intensity to the native protein,[4] where the extinction coefficients are ($\varepsilon_{470} = 1.600\ mM^{-1}\ cm^{-1}$), ($\varepsilon_{593} = 6.300\ mM^{-1}cm^{-1}$), ($\varepsilon_{770} = 3.000\ mM^{-1}\ cm^{-1}$), the 470 nm peak is considerably less intense. The spectrum of D92N has been reported previously[23] and again shows an absorbance at 460 nm ($\varepsilon_{460} = 0.950\ mM^{-1}\ cm^{-1}$) and a stronger absorbance at 595 nm ($\varepsilon_{595} = 4.700\ mM^{-1}\ cm^{-1}$). In all three cases the absorbance peak at 600 nm is typical for a T1Cu centre.

Electron paramagnetic resonance (EPR)

Figure 1 shows the EPR spectra of the three mutants. M144A clearly shows that both T1Cu and T2Cu are present. The spectrum is significantly more complex compared to the H254F and D92N enzymes, where only the T1Cu signals are detected (see below). The hyperfine splitting for the T1Cu in M144A is subsumed by the T2Cu signal. The mutation at the type 1 Cu site, M144, causes shifts in the type 1 peaks resulting in broad features which proved impossible to simulate. As such, difference calculations could not be performed. Despite the broader features, the binding of nitrite is detectable in the EPR spectrum where there is a significant shift in the features attributable to the T2Cu (data not shown).

The EPR spectrum of H254F shows hyperfine splitting indicative of a T1Cu site. The simulated EPR parameters are $g_{\perp} = 2.04$, $g_z = 2.23$, $A_{\perp} = 0.5$ mT and $A_z = 6.0$ mT. There was no T2Cu hyperfine splitting detected even in the presence of an excess of K_2FeCl_6 suggesting that the lack of T2Cu signal is not due to Cu being in the reduced state. Addition of excess sodium nitrite did not cause any change in the EPR spectrum.

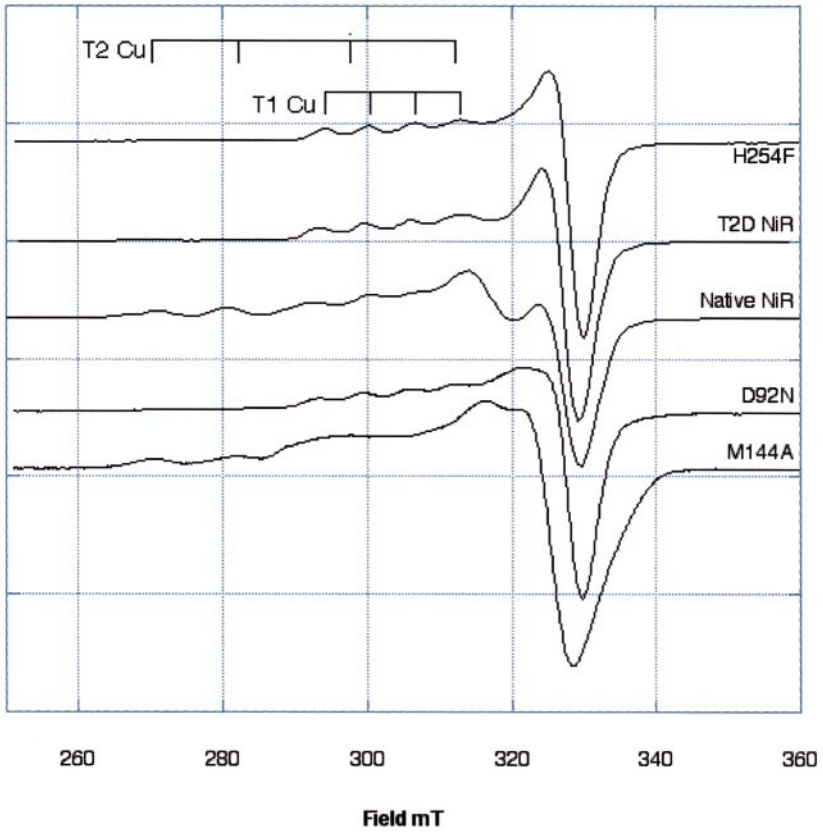

Figure 1. The EPR of M144A is a complex signal involving both T1 and T2Cu centres. Both H254F and D92N show only the T1Cu signal. The EPR of native NiR, T2D native NiR and D92N have been reported previously and are here as a comparison.

The spectrum of D92N has been published but is added here for comparison.[23] D92N exhibits typical T1Cu hyperfine splitting ($g_\perp = 2.045$, $g_z = 2.215$, $A_\perp = 0.0$ mT and $A_z = 6.5$ mT). In this case the T2Cu signal was not detectable in the resting enzyme. However, this changes upon addition of nitrite when a weak T2Cu signal was detected, there was also a change in the signal from an axial to rhombic form for the T1Cu ($g_x = 2.12$, $g_y = 2.13$, $g_z = 2.41$, $A_x = 0.0$ mT, $A_y = 4.6$ mT, $A_z = 12.5$ mT). It was concluded that there was some T2Cu present and that the mutation was increasing the reduction potential of the T2Cu and therefore only a T1Cu signal was detected. Addition of K_2FeCl_6 was used to oxidise the protein and a weak T2 signal was detected indicating there was T2Cu present but mainly in a reduced state.[23]

The T1Cu signals of D92N and H254F are very similar to the recombinant protein where the simulated T1Cu signal has been determined to be $g_\perp = 2.11$, $g_z = 2.29$, $A_\perp = 0.0$ mT and $A_z = 6.4$ mT.[15]

Enzyme activity and redox potential

Table 1 provides the results of activity measurements conducted on the three mutants. The electron donor, methyl viologen has been used. Both H254F and D92N show no activity. M144A maintains a level of ~30 % of the activity compared to the native enzyme. The redox potential of M144A was found to be 314(±5) mV compared to 240 mV measured for the native enzyme.

X-Ray fluorescence (XRF)

X-ray fluorescence data were obtained using synchrotron X-rays on the same protein samples as used for crystallisation and spectroscopic studies. These data have been normalised to the scattered intensity at 12 keV and provide a relative metal content of the samples (Figure 2). These data show that each of the samples contain a similar amount of Zn but the Cu content differs with M144A exhibiting the highest Cu level while H254F shows the lowest Cu level reducing to a level similar to Zn. The Zn content is similar to levels found previously for the wild-type and T2D (native protein with T1Cu only) enzyme.[24] The Cu peak of M144A is of similar height to the native, suggesting that both metal sites are occupied by Cu.

Table 1. % Activity relative to recombinant NiR

Sample	Methyl viologen
M144A	31.5±4.5
D92N	0.05±0.01
H254F	0.0

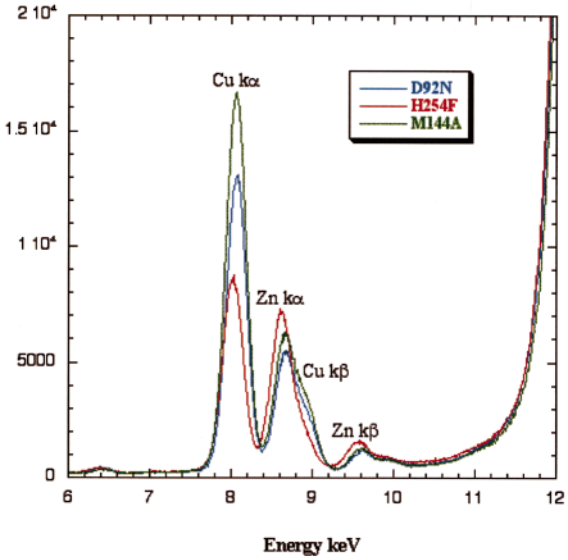

Figure 2. The XRF plot of M144A (green), D92N (blue) and H254F (red) clearly shows the relatively low Cu:Zn ratio of H254F. Calculation of area under the Zn K_α peak was complicated by the overlap of the CuK_β peak.

EXAFS studies show T2Cu replaced with Zn in H254F

The lack of a T2Cu signal in the EPR spectrum of H254F and the Cu:Zn ratio of 1:1 from XRF studies of the protein suggested further analysis was needed. To shed light on the nature of both Cu and Zn present in the sample, EXAFS data were collected at the Cu and Zn edges. Comparison of the k^3 weighted Cu *k*-edge of H254F and native T2D NiR suggests that the Cu is in a site typical of a T1Cu (Figure 3(a)), thus confirming of the results from EPR and suggesting lack of Cu in the T2Cu site.

A comparison of the k^3 weighted Zn *k*-edge EXAFS of H254F (Figure 3(b)) and the k^3 weighted Zn-edge EXAFS of Cu/Zn SOD[25] show close similarity, thus suggesting that the Zn is indeed in the T2Cu site as there is no other site with suitable ligation in the protein where three histidine residues could be provided.

Substitution of Cu with Zn is not unknown. In the mutation M150E[20] of *Af*NIR (equivalent to M144E in *Ax*NiR) the T1Cu is replaced by Zn. However in this case there was no Zn detected in the T2Cu site. The loss of T2Cu has been noted before, specifically with mutations of *Rhodobacter sphaeroides* NiR[26] where the estimated copper content of some mutations was 1 Cu per monomer. However, in this case, there is no indication of estimated Zn content.

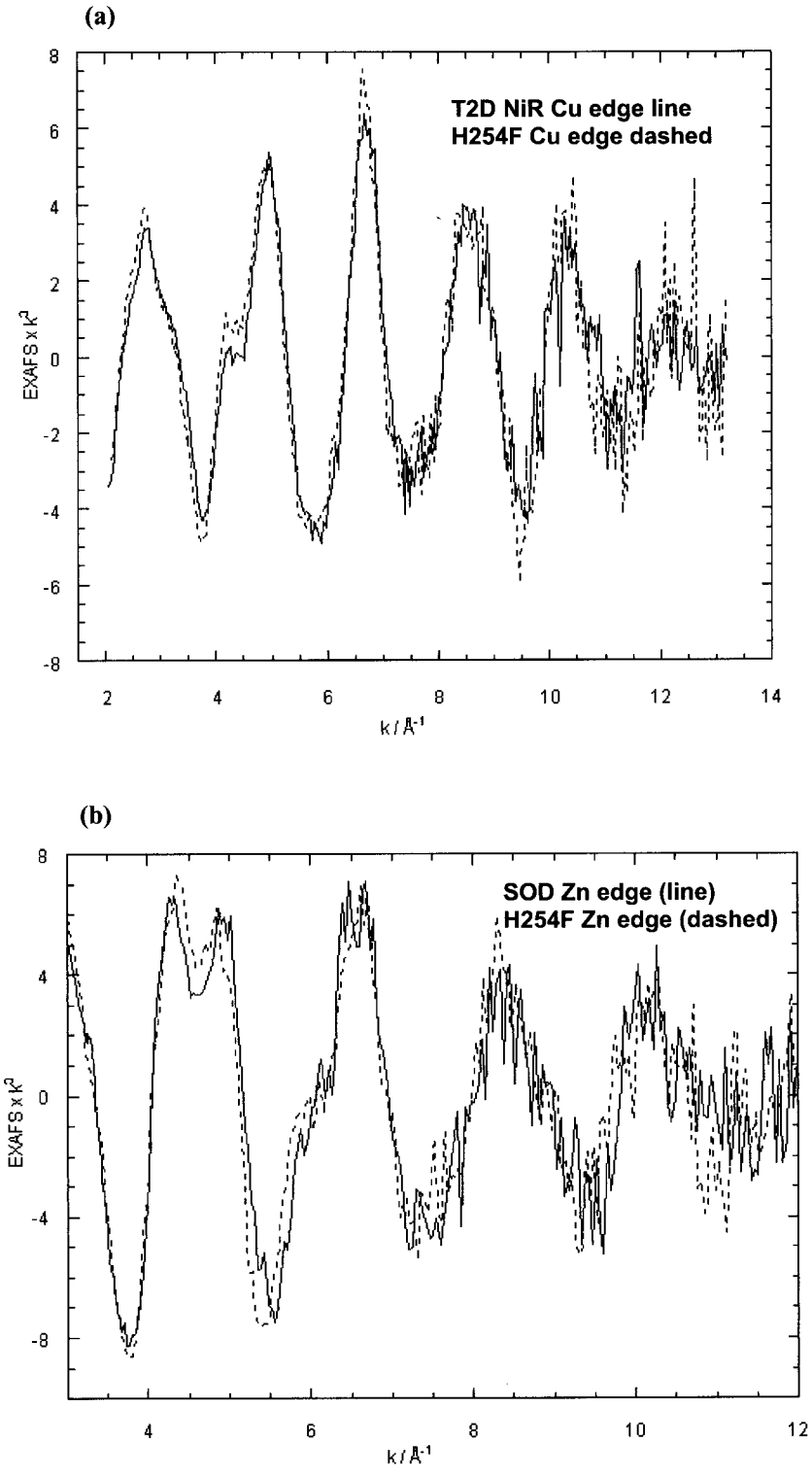

Figure 3. Comparison of the k^3 weighted Cu *k*-edge EXAFS of H254F NiR and the T2D native *Ax*NiR show close structural similarity (a). The k^3 weighted Zn *k*-edge EXAFS of H254F NiR and the Zn *k*-edge of Cu/Zn SOD (b) suggests at least three histidine residues ligating a Zn in H254F.

Does H254F exhibit carbonic anhydrase activity ?

The T2Cu site in native NiR has been shown to be structurally similar to a site found in Zn enzymes including carbonic anhydrase.[24] The carbonic anhydrase activity measurements of H254F showed that the protein is inactive. This would seem to suggest that while the two systems are structurally similar, they have significant differences in their reaction mechanisms and that there are other structural features outside the metal sites which are important for substrate utilisation.

General comparison of the structures of the mutants with the native protein

The overall structures of D92N, M144A and H254F are trimeric, as in the native protein. Superposition of the Cu sites of the mutants with the native protein has shown differences in the environment around both the type 1 and type 2 Cu sites. RMS deviations for M144A and D92N compared to the native protein are 0.24 and 0.22 Å, respectively. There is a larger difference when H254F is compared to the native structure (0.36 Å). All three mutants have metals (Mg for M144A and Zn for D92N and H254F) bound to the surface of the protein. This is in contrast to the native protein where only the type 1 and type 2 Cu centres are seen and no surface binding sites have been identified.

Overall the *B*-factors on individual atoms in M144A are significantly higher than in the native protein. Values for the Cruickshank DPI (ESU based on *R*-value) and the *B*-factor ESU (Table 2) are higher for the M144A structure in comparison to either D92N or H254F. This is reasonable due to the lower resolution (2.2 Å) of the structure of the M144A mutant.

The T1Cu sites

Even though the XRF data of M144A by comparison to the native enzyme suggest that both sites are fully occupied by Cu, the type 1 metal has been modelled with 50 % occupancy based on the $F_o - F_c$ map. The full occupancy Cu results in considerably higher B (>40 Å^2) compared to the ligating atoms which show an average B of 30 Å^2. This could suggest that Cu is significantly disordered and probably partially reduced. With the 0.3 Å movement of the Cu, His139 has also moved by 0.3 Å away from the cavity, however the distance between Cu and His139N$^{\delta 1}$ has remained similar (change of 0.07 Å, see Table 3 and Figure 4(a)). Finally, there has been a slight (0.1 Å) increase of the Cu-Cys130S$^{\gamma}$ separation, which has caused a slight expansion of the site.

As observed for the M144A structure there are subtle changes in the residues ligating the Cu sites in the D92N structure. At the T1Cu site (Figure 4) there is a movement of ~0.2 Å of His139 away from the Cu. Aside from a slight movement of C$^{\beta}$ in the Cys130 residue there are no significant changes in either Met144 or Cys130 with this residue. In H254F the biggest changes are in the movement of 0.15 Å of the Met S$^{\delta}$ towards the Cu. There is also movement (0.15 Å) of the His89 imidazole away from the Cu site (Figure 4(a)).

The T2Cu sites

The differences at the type 2 Cu site of M144A are less marked than at the T1Cu site (Figure 4(b)). The *B*-factors at the T2Cu are comparable to those of the native protein. His129 has shifted away from the Cu centre by ~0.2 Å. The position and distance of His94 in relation to the Cu has remained the same. HisB249 has moved away (0.1 Å) from the Cu centre opening the cavity

Table 2. Summary of X-ray data and model qualities for the M144A, H254F and D92N mutants

	M144A	H254F	D92N
A. *Data quality*			
Space group	$P6_3$	$P6_3$	$P6_3$
Resolution (Å)	2.2	1.85	1.9
Unit cell (Å)	$a = b = 106.9$, $c = 63.0$	$a = b = 79.7$, $c = 99.9$	$a = b = 79.7$, $c = 99.9$
Observed reflections	80,145	252,101	185,774
Unique reflections	27,656	29,614	35,114
Completeness (%)	99.4(99.4)[a]	98.5(97.2)	100(100)
R_{merge} (%)	9.7(32)	5.9(33.1)	8.4(27.2)
I/σ (I)	11.2(2.4)	13.9(2.4)	12.9(4.3)
R_{work} (%)	17.1	17.8	17.1
R_{free} (%)	21.0	22.1	20.7
B. *Model quality*			
B-factors:			
Wilson (Å^2)	21.5	19.0	16.5
Protein (Å^2)	31.0	19.3	17.2
Water (Å^2)	40.5	28.2	26.0
Cruickshank DPI (Positional ESU)	0.19	0.13	0.13
B-factor ESU based on ML	3.29	2.02	2.02
RMS deviations:			
Bond distances (Å)	0.013	0.016	0.016
Overall ESU: Cruickshank DPI	0.20	0.13	0.14
Ramachandran plot (non-Gly, non-Pro)			
Residues in most favoured regions (%)	88.9	90.1	90.5
Residues in additional allowed regions (%)	11.1	99.9	9.5
PDB entry code	1GS6	1GS7	1GS8

[a] Values in parentheses are for outer resolution shell, 2.32 to 2.20 Å for M144A, 1.88 to 1.85 Å for H254F and 1.97 to 1.90 Å for D92N.

Table 3. Cu-ligand distances of native, M144A, H254F and D92N

Atom 1	Atom 2	Distance in native (Å)	Distance in M144A (Å)	Distance in H254F (Å)[a]	Distance in D92N (Å)
T1Cu	His89 $N^{\delta1}$	2.0	2.1	2.2	2.2
T1Cu	Cys130 S^{γ}	2.2	2.3	2.2	2.2
T1Cu	His139 $N^{\delta1}$	2.0	2.0	2.1	2.1
T1Cu	Met144(Ala)* $S^{\gamma}(C^{\beta})$*	2.7	5.0	2.6	2.6
T2Cu	His94 $N^{\varepsilon2}$	2.0	2.0	2.0	2.1
T2Cu	His129 $N^{\varepsilon2}$	2.0	2.2	2.0	2.1
T2Cu	His B249 $N^{\varepsilon2}$	3.6	3.7	3.7	4.0
T2Cu	His B300 $N^{\varepsilon2}$	2.3	2.2	2.1	2.2
T2Cu	Wat 503	1.7	1.9	2.1	2.3
Wat503	Asp92(Asn)# $O^{\delta2}(N^{\delta2})$#	2.5	2.6	2.7	3.1
Wat600	Asp92(Asn)# $O^{\delta1}$	2.7	2.7	2.8	2.8

Parentheses indicate M144A (*) and D92N (#) mutations.
[a] T2Cu site distances are from the Zn atom.

slightly. HisB300 has remained in the same position.

In D92N the differences are more marked, the replacement of $O^{\delta2}$ with $N^{\delta2}$ has had several effects. Primarily the position of the Cu ligating water molecule has been significantly altered. It has moved some 1.5 Å around the Cu towards HisB300. This is consistent with the findings of Boulanger *et al*.[21] However there is not the reorientation of residue 92 seen in *Af*NiR. The position of the water at the end of the proton channel, W600, has not changed. There are slight movements in the histidine residues ligating the T2Cu. HisB300 and HisB249 have moved slightly outwards, opening up the cavity. His129 has also moved away from the Cu site by ~0.17 Å.

The changes of H254F at the T2Cu site are marked. Omitting metal from the modelled T2Cu site generates a large peak in the $F_o - F_c$ map, suggesting that a metal should be present. The lack of the T2 EPR signal, and the XRF results indicate a higher amount of Zn suggesting that at least some of the Cu in the T2Cu site has been replaced by Zn. Further confirmation for the replacement of the T2Cu with Zn came from EXAFS measurements. These data showed the presence of a T1Cu centre (Figure 3(a)) and absence of T2Cu signal. Furthermore, the Zn edge EXAFS data were similar to the Zn site of bovine Cu/Zn SOD (Figure 3(b))

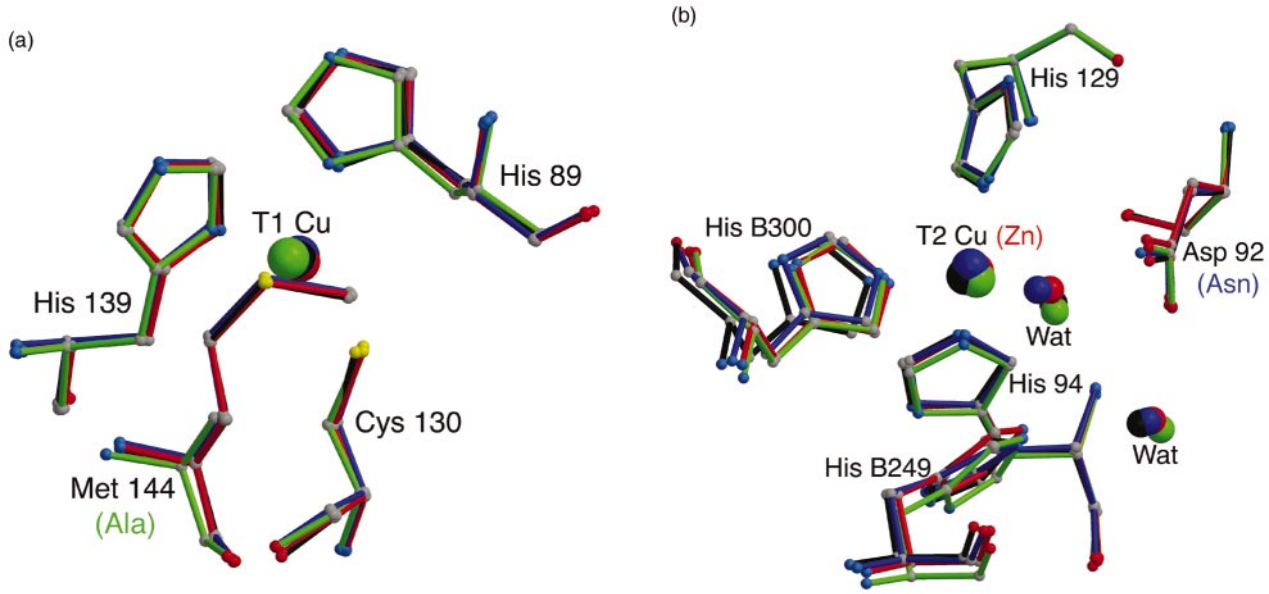

Figure 4. (a) The T1 Cu sites of M144A (green), D92N (blue) and H254F (red) with the native protein (black) show little difference in the position of any of the ligating residues. (b) Differences are clearly visible at the T2Cu sites of M144A (green), D92N (blue) and H254F (red) in comparison to the native protein (black). There is a clear movement in the position of the Cu-ligating water, with the greatest movement of ~2 Å in the position of the D92N water. In all three mutants His300 from the second subunit has moved closer to the Cu. The D92N mutation has the $N^{\delta2}$ atom pointing towards the Cu-ligating water. NH_2 is a weak proton acceptor/donator ligand and is not able to transfer protons to the active site. Figures 4, 5, 6 and 7(d) were generated using Molscript[44] and Raster3D.[45]

strongly suggesting that the T2Cu site was occupied by Zn.[25] A full occupancy Zn in this site provides a reasonable *B*-factor (14.62 Å^2), suggesting that the T2Cu site is indeed occupied by Zn. While there are no significant movements in His129, His249 or His94 there is a movement of 0.2 Å of His 300 towards the metal centre. The distance of the water ligating the metal centre is increased significantly over the native protein (~0.4 Å). This is slightly less than the movement seen for this water molecule in D92N. The position of the $O^{\delta 2}$ oxygen of Asp92 is such that the distance to the Cu ligating water molecule has increased to 2.72 Å and this is again about half way between the value obtained for the native and D92N mutant. The water molecule (W600) which hydrogen bonds to Asp92 $O^{\delta 1}$ and leads into the proposed water channel resides 2.82 Å away from the Asp92 $O^{\delta 1}$ and is similar in distance to the same atoms in D92N (Figure 4(b)).

Perturbation of T1Cu by loss of Met144

Truncation of Met144 to Ala has had the effect of removing the weak axial ligand from the T1Cu site (Figure 4(a)). The C^{β} of alanine is situated 5 Å away from the T1Cu and is therefore outside its co-ordination sphere. The loss of Met144 coincides with 70 % reduction in enzyme activity indicating that the T1Cu site has been perturbed. The redox potential of the type 1 Cu centre is known to modify by up to 100 mV when methionine is mutated or removed altogether.[16,27,28] In the case of Azurin when the methionine is mutated to an alanine, the redox potential is increased by about 60 mV.[28–30] In our case, M144A mutant results in an increased redox potential of 74 mV (mutant 314 mV *versus* native 240 mV). For M144A this would lead to an increased energy barrier for transferring an electron from the T1Cu to the T2Cu thus reducing the activity of the enzyme.

The proton channel of H254F

Analysis of the proton donation channel in which His254 resides shows that there is a breakdown in the hydrogen bonded network at Phe254 (Figure 5). The loss of the side-chain nitrogen atoms from the His group has allowed the WatA to move to a more favourable position for hydrogen bonding to Tyr287. This movement of water molecules has had an effect further towards the T2 site where the WatB, hydrogen-bonded to His94 O, has moved upwards and no longer hydrogen bonds to the WatC at Asp92. This disrupts the proton channel from what is believed to be the proton abstracting group.

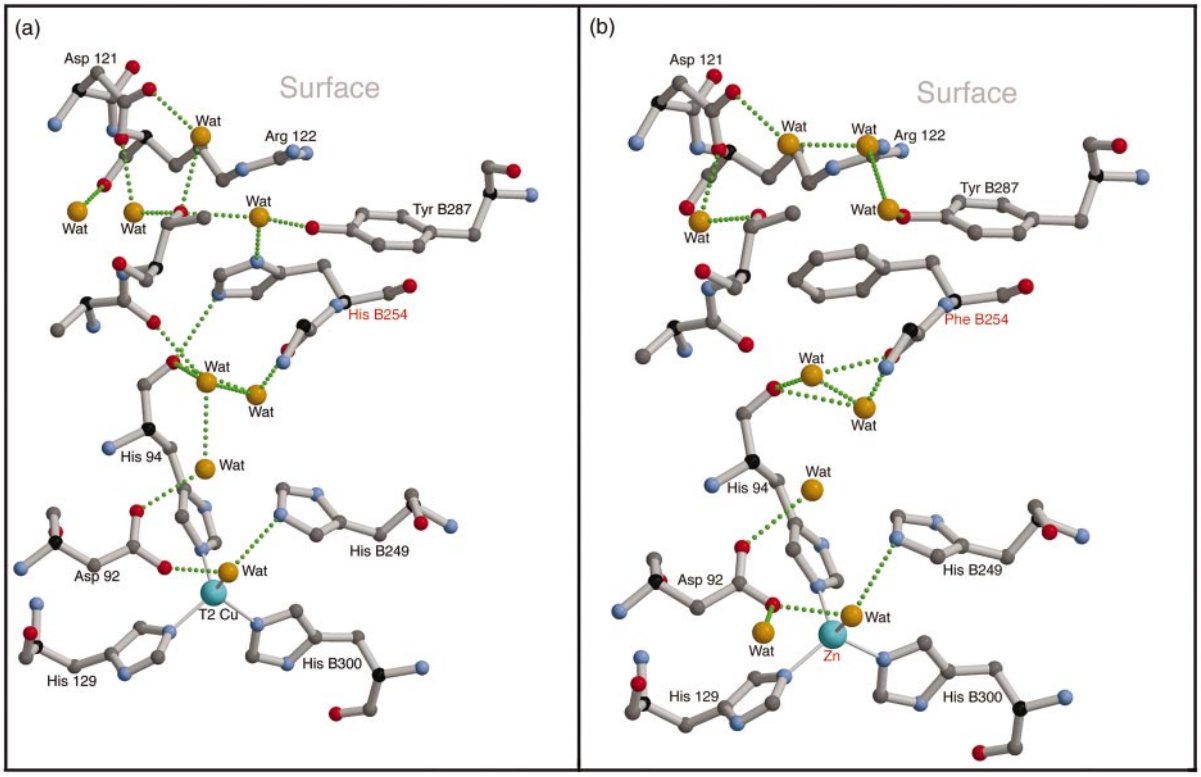

Figure 5. The water network of the native protein (a) and the H254F mutant (b) is very similar. The break of the hydrogen-bonded network at Phe254 is clear.

Is the T2Cu site of D92N *Ax*NiR comparable to the T2Cu site of D98N *Af*NiR?

Recent studies of the Asp98 mutations of *Af*NiR, the *Ax*NiR Asp92 equivalent, have allowed some insight into the function of the ligands surrounding T2Cu site.[21] In the crystal structure of D98N from *Af*NiR, the side-chain of Asn98 was shown to be rotated by 40° leading to a 1 Å movement of the $N^{\delta 2}$ atom away from the position of the Asp $O^{\delta 2}$ atom in native *Af*NiR. This also leads to a movement of $N^{\delta 1}$ away from the ligating water.

In contrast, there is no reorientation of the Asn side-chain in *Ax*NiR D92N. $N^{\delta 2}$ is in the same position as the $O^{\delta 1}$ atom of Asp92 in the native protein. The significant movement of the Cu-ligating water molecule has been put down to the fact that the $N^{\delta 2}$ group is a weak proton acceptor ligand thus the water molecule is free to move to a more favourable position. The rotation of N98 in *Af*NiR results in the lengthening of the hydrogen bond to the water leading into the proton channel. Again this is not the case in *Ax*NiR D92N, where the water resides in the same position as in the native protein and hydrogen-bonds to Asn98 (Figure 4(b)).

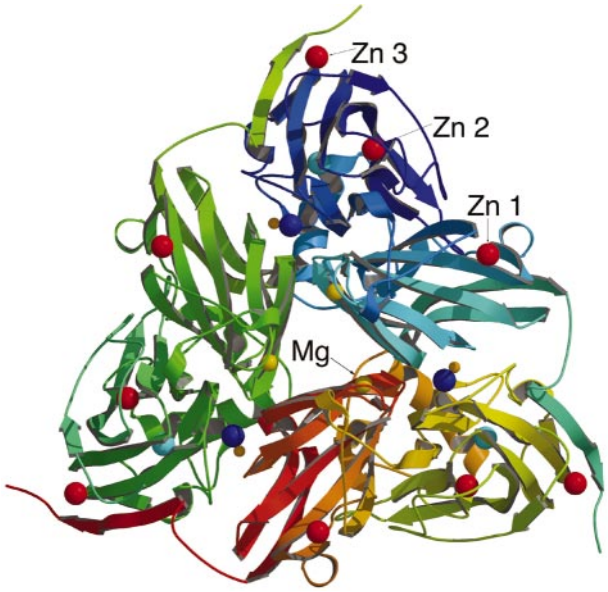

Figure 6. The positions of the Zn and Mg sinks on the surface of the protein are clearly defined. Looking at the trimer of *Ax*NiR, the position of Zn1 is some 21 Å from Zn2, which lies 14 Å from Zn3. The Mg binds to the inside surface of the trimer.

Zn sinks

Despite the close similarity of T2Cu site of copper nitrite reductases to the Zn site of carbonic anhydrases, it has remained a puzzle why despite the availability of Zn little or no Zn makes it to the Cu site of NiR. Observation of a number of Zn binding sites on the surface of the enzyme would suggest that the enzymes has provision for scavanging this metal.

The D92N mutant contains several metals on the surface of the protein. The sites have been modelled with partial occupancy zinc atoms since this was the only cation present during crystallisation in any significant concentration (10 mM). There are three surface binding sites in D92N, two contain 75% occupancy zinc atoms, Zn601 and Zn602. The final zinc has 50% occupancy, Zn603 (Table 4 and Figures 6 and 7(a)-(c)). Both Zn601 and Zn602 are co-ordinated by a His, an Asp and two water molecules (Figure 7(a) and (b)). Zn603 has long range interactions with an Asp, Leu and His but no water molecules can be seen ligating Zn603 (Figure 7(c)) at our current resolution. The major difference between Zn603 and either Zn601 or 602 is that the Asp side-chain is free, preferentially pointing away from the binding site, thus the site would seem to bind more weakly.

H254F contains a single metal on the surface of the protein. The site has been modelled with a partial occupancy (75%) zinc atom since the crystals were grown in the presence of the metal. The sur-

Table 4. Surface metal-ligand distances in D92N, H254F and M144A

Metal atom	Ligand atom	D92N Distance (Å)	H254F Distance (Å)	M144A Distance (Å)
Zn601 (Mg601)	His165 $N^{\varepsilon 2}$ (Glu260 O)	2.2	2.1	2.8
Zn601 (Mg601)	Asp167 $O^{\delta 1}$ (Arg278 N)	2.8	2.8	3.0
Zn601 (Mg601)	Asp167 $O^{\delta 2}$ (Arg278 NH1)	2.1	2.0	3.1
Zn601 (Mg601)	Wat791 (Ser 281 O^{γ})	2.1	2.1	2.7
Zn601	Wat822	2.4	2.4	
Zn602	His70 $N^{\delta 1}$	2.4		
Zn602	Asp73 $O^{\delta 1}$	3.4		
Zn602	Asp73 $O^{\delta 2}$	2.1		
Zn602	Wat630	2.4		
Zn602	Wat788	1.9		
Zn603	Asp4 O	3.6		
Zn603	Leu6 O	4.3		
Zn603	His8 $N^{\varepsilon 2}$	2.0		

Atoms in parenthesis are for the mutation M144A.

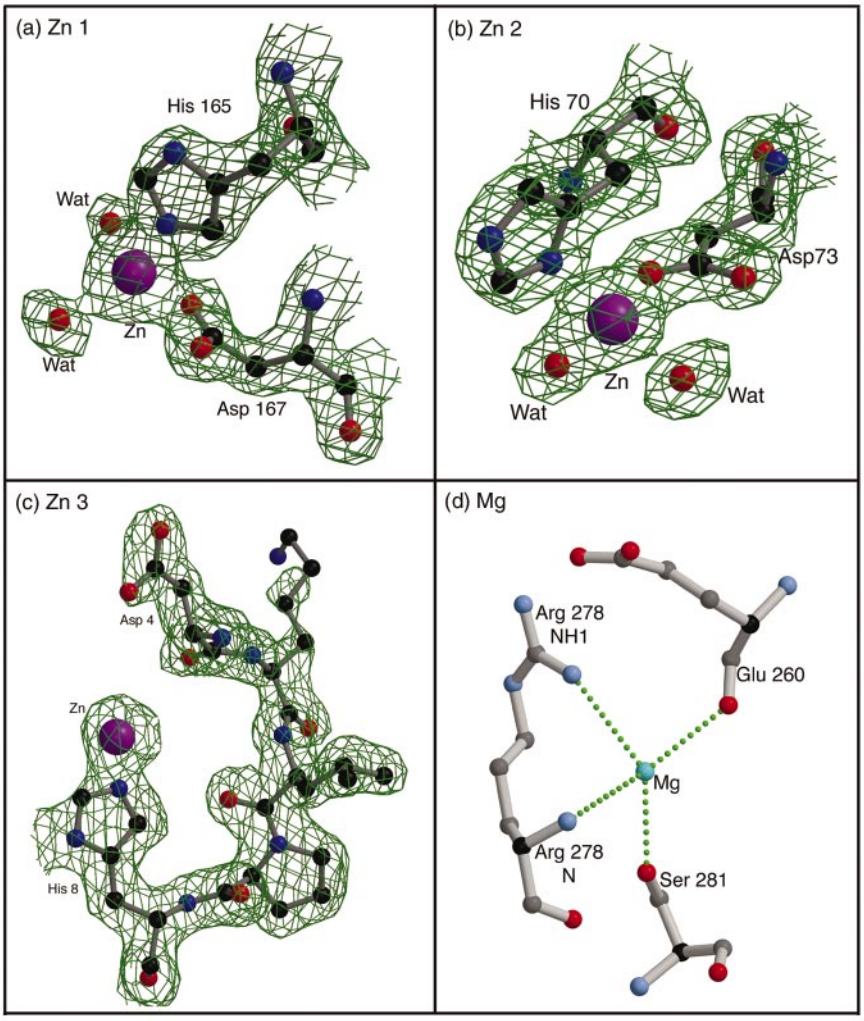

Figure 7. The position of the surface Zn and Mg ion binding sites (see Figure 6) are clearly located in the $2F_o - F_c$ map. Asp and His residues are involved in all three Zn binding sites. However in Zn3 (c) the Asp side-chain is pointing away from the metal. Zn1 is conserved in both the structures of H254F and D92N. The maps were created at 1.75 σ, 1.75 σ and 1.5σ, respectively. (a), (b) and (c) were generated using Bobscript.[46]

face Zn is co-ordinated by His165, Asp167 and two water molecules. Interestingly the Zn is in the same position as Zn601 of the D92N mutation.

All three Zn sites lie approximately in a straight line down the long axis of the trimer (Figure 6). The distance between Zn601 and Zn602 is ~21 Å with Zn603 a further 14 Å from Zn602. The similarity in binding site would seem to suggest that the Asp-His site is good at scavenging Zn atoms from the surrounding environment. This suggests that ''free'' zinc which is present in the solvent readily binds in these positions in preference to the T2Cu site, which is buried after trimerisation. None of the Zn sites were occupied in the case of M144A where $ZnSO_4$ was absent from the crystallisation medium.

Additional metal binding sites

In M144A magnesium (Mg) is bound to the internal surface of the protein trimer (see Figure 6). It is weakly bound by four atoms from three residues Glu260, Arg278 and Ser281 (Table 4, Figures 6 and 7(d)). The *B*-factor for the Mg atom is similar to those of the surrounding residues, indicating that it is a full occupancy metal. The presence of metal is not unexpected due to the levels of Mg present in the crystallisation conditions (see Materials and Methods). However the position, on the inside surface of the protein, would not appear to be favourable due to steric effects from the bulk of the protein and the proximity of the other subunits in the trimeric structure.

Conclusions

Structure-function relationship has been investigated for copper nitrite reductase by combining biochemical, spectroscopic and crystallographic studies of point mutated enzyme. The small alteration at the type 1 Cu site caused by point mutation of the weakest ligand methionine causes a

reduction in the enzymatic activity of more than 50 %. This demonstrates that slight alteration in redox potential (~70 mV increase), results in a less effective electron transfer from the type 1 Cu centre to the type 2 Cu centre which is the site of nitrite utilisation. The combined study of this mutant also provides strong support to the idea that electrons are mediated *via* the type 1 Cu centre and that status of the two metal centres is communicated *via* the His129-Cys130 and Asp92-His89 links.[11,31]

Analysis of the hydrogen bonded water network in H254F shows that there is a break down in the hydrogen bonds at the mutation site. There is no longer a direct network of hydrogen bonded water molecules from the T2Cu to the surface of the protein. Removal of the histidine nitrogen atoms has allowed the previously hydrogen bonded water molecules to move further undermining the stability of the water network. The EXAFS clearly indicate the presence of Zn in the T2Cu site, thus explaining the complete loss of activity in this mutation. However, even though the new site is structurally similar to carbonic anhydrase, assays of the carbonic anhydrase activity of the mutant show H254F to be inactive, suggesting clearly that structural aspects beyond the metal site are important for the substrate utilisation.

The equivalent mutation to D92N in *Ax*NiR is D98N in *Af*NiR.[21] There is a significant difference in the rotation of the N92 side-chain in D92N. It has been reported that N98 rotates by ~40° in D98N. There is little to no movement in D92N and a lack of hydrogen bonding to the Cu-ligating water is considered to be due to the $N^{\delta 2}$ atom of Asn92 being a proton acceptor ligand and not a proton donator.

M144A has a Mg ion just under the surface of the protein near the trimeric axis. The position of this site is unusual due to the low probability of getting a metal ion so far inside the protein. Both H254F and D92N have Zn atoms bound to the protein surface. It would seem that the general group Asp-(x)-His is able to act as an effective binding site for Zn. We suggest that the position of these groups on the surface of the protein puts them in an ideal position to capture any available Zn ions, thus preventing Zn from occupying the T2Cu site whose geometry is well suited to bind Zn as demonstrated by the H254F structure. In the case of H254F mutant Zn is able to get to the T2Cu site probably because the amount of Zn available has been high.

Materials and Methods

Bacterial strains and plasmids

The *Escherichia coli* strains used in this study were JM109 F′ *tra*D36 *lacI*^{q} Δ(*lac*Z)*M15 proA*$^+$*B*$^+$/e14$^-$(McrA$^-$) Δ(*lac-pro*AB) *thi gyr*A96(Nal^r) *endA1 hsd*R17 ($r_K^-m_K^+$) *relA1 supE44 recA1*,[32] BL21(DE3) F$^-$ *ompT gal {dcm} {lon} hsdSB* ($r_B^-m_B^-$; an *E. coli* B strain) with DE3, a λ prophage carrying the T7 RNA polymerase gene[33], and *E. coli* XL1-Blue (Stratagene). The plasmids used in this study were pUC18 and pUC19 (ApR),[32] pBR322 (ApR)[34] and pET28a (KanR) (Novagen), and pEnirsp-1, which is similar to pET28a but includes the *A. xylosoxidans nirA* gene under the control of the phage T7 f10 gene promoter.[15] Antibiotics were used at a final concentration of 50 mg ml^{-1}.

Bacteria were grown routinely in Luria Broth (LB) (1 % (w/v), B-actotryptone (Difco), 0.5 % (w/v) yeast extract (Difco), 1 % (w/v) NaCl) at 37 °C. Small-scale cultures (up to 10 ml) for plasmid DNA isolation were grown aerobically in sterile conical flasks filled to approximately 10 % of their volume with growth medium. Large-scale growths (20 l or 200 l) used for isolation of NiR were cultured in New Brunswick fermentors under the control of Bio-Command software, with 20 % air saturation. Media were supplemented with $CuSO_4$ (1 mM) and the appropriate antibiotic solution. Antibiotics were purchased from Sigma and stock solutions were prepared in water and filter sterilized through sterile 0.2 mm syringe filters (Sartorius). Induction of high level protein production was initiated when the cultures had reached late exponential phase of growth, through the addition of 0.5 mM isopropyl-β-D-thiogalactopyranoside (IPTG) and 0.4 % (w/v) glucose. Growth was continued for a further 90 minutes after which time the cells were harvested by centrifugation. Cells were used immediately for the isolation of NiR or were stored frozen at −80 °C until required.

Site-directed mutagenesis of the *nirA* gene

Site-directed mutagenesis of the *nirA* gene in plasmid vector pEnirsp-1[15] was performed with the QuikChange Site Directed Mutagenesis Kit (Stratagene), following the instructions of the manufacturer. The oligonucleotides used to construct the *nirA* gene mutants for M144A were M144A-F(5′-GTGGTGTCGGGCGCGAGCGGCAC GCTG-3′), and M144A-R(5′-CAGCGTGCCGCTCGC GCCCGACACCAC-3′), for H254F the oligonucleotides were H254F-F(5′-GATCGGCGGCTTTGGAGACTGGGTT TGG-3′) and H254F-R(5′-CCAAACCCAGTCTCCAA AGCCGCCGATC-3′). The resulting plasmids were termed pEnirM144A and pEnirH254F, which encoded the NiR mutant M144A and H254F respectively. The complete DNA sequences of the mutant *nirA* genes were verified using the method of Sanger *et al*.[35]

Biochemistry of Met144Ala and His254Phe

The M144A and H254F mutant forms of AxNiR were purified from periplasmic extracts of recombinant *E. coli* cells as described by Prudêncio *et al*.[15] The periplasmic fraction of the mutants were dialysed against 1 mM $CuSO_4$, before purification.

EPR

EPR spectra for M144A D92N were collected at −150 K with a frequency of 9.41 GHz and 9.40 GHz, respectively, and a microwave power of 20 W, using a Bruker ER ER200 D-SRC spectrometer fitted with an ER042 MRH microwave bridge with an ER033C field frequency lock and an Oxford Instruments Ite^{503} temperature controller. EPR spectra were simulated with the program WINEPR-SimFonia (Bruker), Spin quantifications were made as described by Åasa and Vänngård.[36]

EPR for H254F were collected at 100 K with a microwave power of 4 W, a frequency of 9.125 GHz with a JEOL FES-RE2X spectrometer fitted with a JEOL X-Band microwave bridge and a JEOL DVT2 temperature control unit. EPR spectra were simulated with the in-house program EPRSIM (Strange, unpublished).

Substrate binding to Met144Ala and His254Phe monitored by EPR

The substrate binding ability of M144A was analysed by EPR. The protein was incubated with a 20-fold molar excess of nitrite over the estimated type 2 Cu content and the EPR spectrum was recorded. H254F was incubated with a 20-fold molar excess of nitrite over the estimated protein concentration and the EPR spectrum was recorded.

Spectroscopic methods

UV/Vis spectra were collected on either a Hewlett-Packard 8452A diode array (M144A/D92N) or Perkin Elmer Lambda 18 (H254F) spectrophotometer.

Enzyme activity assays

NiR activity was determined using three independent methods. The discontinuous methyl viologen assay was performed as described by MacGregor[37] and Abraham *et al*.[4] The reaction mixture contained in a final volume of 2 ml, 250 mM potassium phosphate buffer (pH 7.1), and 0.1 mM sodium nitrite. Methyl viologen (MV) at a concentration of 0.5 mg ml^{-1} was used as the electron donor and the reaction was initiated by the addition of dithionite to a final concentration of 0.4 mg ml^{-1} followed by gentle mixing. The mixture was then incubated at 25 °C for five minutes and the reaction was stopped by vortexing to oxidise the residual dithionite. The amount of nitrite left in the reaction mixture was then determined from the UV/Vis spectra. One unit of enzyme activity is defined as the reduction of 1 μmol of nitrite per minute per mg of protein. Redox potentials for native and M144A mutants were measured spectrophotometrically using the blue absorption band.

Electrophoresis of proteins

Gel electrophoresis (SDS-PAGE) was used routinely to check the purity of protein samples throughout the purification of NiR and to check overproduction levels of recombinant NiR proteins. SDS-PAGE was performed as described by Laemmli.[38] Typically, 12.5 % (w/v) or 15 % (w/v) acrylamide gels were run. For whole cell extracts, the $A_{600\ nm}$ was measured and a volume of $1.2/A_{600\ nm}$ (in ml) of cell suspension was centrifuged and the cell pellet resuspended in 80 ml of SDS sample buffer.

Determination of protein concentration

Protein determinations were done by the method of Lowry *et al*.[39] For pure preparations of NiR the protein concentration was also estimated using an extinction coefficient at 280 nm of 1.54 M^{-1} cm^{-1} (R.E., unpublished results).

XRF sample preparation and data collection

Oxidised samples of the protein were buffer exchanged into 0.1 M Mes (pH 6.5), the same buffer and pH as the crystallisation conditions. Samples were then loaded into EXAFS cells and immediately frozen in liquid nitrogen.

XRF were collected on Station 9.2 at the SRS, Daresbury Laboratory. A solid state 13 element (Canberra) Ge fluorescence detector was used. XRF studies carried out on the three mutations give a rapid and accurate assessment of the metal content of the sample. Data were collected with the signal optimised at the CuK_α edge. The ratio of Cu:Zn in each of the samples was calculated from the area under the Cu and ZnK_α peaks.

Protein crystallisation

Thin colourless crystals of Met144Ala were grown using the sitting drop vapour diffusion method using a 1 ml reservoir comprising of 30 % PEG 4000, 0.1 M $MgCl_2$, 0.1 M Tris-HCl (pH 8.5). The temperature was increased at a constant rate from 4 to 32 °C over a three day period. The drop consisted of 3 μl protein solution and 3 μl reservoir solution. The initial protein concentration was 5 mg ml^{-1} in Tris-HCl (pH 7.1).

Small blue hexagonal crystals of D92N and H254F were grown using the sitting drop vapour diffusion method at 21 °C using a 500 μl reservoir comprising of 40-50 % PEG-MME 550, 10 mM $ZnSO_4$, 2 mM $NaNO_2$, 0.1 M Mes (pH 6.5). The drop consisted of 2 μl protein solution and 2 μl reservoir solution. The protein was at an initial concentration of 11 mg ml^{-1} in 10 mM Tris-HCl (pH 7.1). Microseeds of another NiR mutant were used as nucleation centres. Crystals grew within a week to ~0.1 mm × 0.1 mm × 0.08 mm in size and 0.1 mm × 0.1 mm × 1.0 mm respectively.

Data collection and processing for M144A

PX data for the M144A mutant were collected at Station 9.6 at the SRS, Daresbury Laboratory using the ADSC Quantum 4 CCD detector at room temperature using an X-ray wavelength of 0.87 Å. The crystal orientation and data integration were performed using MOSFLM.[40] The data were then scaled and merged using CCP4.[41] Molecular replacement using AMORE[41] yielded an *R*-factor of 23.0 % and correlation coefficient of 87.3 %. The 2.1 Å structure of the native protein[11] (PDB accession code 1NDT) was used as the search model.

The M144A model was subject to a cycle of positional and individual *B*-factor refinement in REFMAC using data from 20.0 to 2.2 Å. This yielded an *R*-factor of 20.3 % (*R*-free 25.5 %). The model consisted of 2524 protein atoms and two Cu atoms. Several cycles of rebuilding of the structure and the inclusion of 100 water molecules yielded an *R*-factor to 17.0 % (*R*-free 21.4 %). The final model consisted of 2572 protein atoms (130 at zero occupancy), 153 water molecules, two Cu atoms and 1 Mg atom and had an *R*-factor of 17.0 %. The Ramachandran[42] plot shows 88.3 % of residues to be in the core regions, with the remaining 11.7 % in the additionally allowed regions (Table 2).

Data collection and processing for D92N

Data for the D92N mutant were collected at Station 9.6 at the SRS using the ADSC Quantum 4 CCD detector. Data were collected at 100 K with the reservoir solution as cryoprotectant. The crystal orientation was determined using the auto-indexing facility in DENZO.[43] Data were scaled and merged using SCALEPACK.[43] Molecular replacement using AMORE[41] yielded an *R*-factor of 28.4 % and a correlation coefficient of 82.1 %.

The D92N model was subject to a cycle of positional and individual *B*-factor refinement in REFMAC[41] using data from 20.0 to 1.9 Å. This yielded an *R*-factor of 22.2 % (*R*-free 26.3 %). The model consisted of 2572 protein atoms and two Cu atoms. A cycle of rebuilding in ''O'' and inclusion of 78 water molecules reduced the *R*-factor to 20.4 % (*R*-free 25.3 %). Further rebuilding of the structure and the inclusion of 177 water molecules yielded an *R*-factor to 16.5 % (*R*-free 20.7 %). The final model consisted of 2572 protein atoms (36 at zero occupancy), 255 water molecules, three Zn atoms and two Cu atoms, *R*-factor 16.5 %. The Ramachandran plot shows 90.5 % of residues to be in the core regions, with the remaining 9.5 % in the additionally allowed regions (Table 2).

Data collection and processing for H254F

Data for the H254F mutant were collected on Station 9.5 again at the SRS using the 165 mm MAR CCD detector. Data were collected at 100 K with the reservoir solution as cryoprotectant. Processing was carried out in a similar fashion to D92N and molecular replacement using AMORE[41] yielded an *R*-factor of 30.6 % and a correlation coefficient of 79.3 %.

The H254F model was subject to a cycle of positional and individual *B*-factor refinement in REFMAC[41] using data from 20.0 to 1.85 Å. This yielded an *R*-factor of 24.9 % (*R*-free 29.8 %). The model consisted of 2567 protein atoms, one Zn atom and one Cu atom. A cycle of rebuilding in O and inclusion of 87 water molecules reduced the *R*-factor to 21.5 % (*R*-free 27.3 %). Further rebuilding of the structure and the inclusion of 150 water molecules yielded an *R*-factor to 17.4 % (*R*-free 22.3 %). The final model consisted of 2581 protein atoms (65 at zero occupancy), 237 water molecules, two Zn atoms and one Cu atom and an *R*-factor of 17.5 % upon inclusion of all data. The Ramachandran plot shows 90.5 % of residues to be in the core regions, with the remaining 9.5 % in the additionally allowed regions (Table 2).

Acknowledgements

The work was supported by CCLRC and by a BBSRC grant (719/B14224) to S.S.H.

References

1. Payne, W. J. (1985). *Dentrification in the Nitrogen Cycle* (Gloterman, H. L., ed.), Plenum Press.
2. Zumft, W. G. (1997). Cell biology and molecular basis of denitrification. *Microbiol. Mol. Biol. Rev.* **61**, 533-616.
3. Kakutani, T., Watanabe, H., Arima, K. & Beppu, T. (1981). Purification and properties of a copper containing nitrite reductase from a denitrifying bacterium, *Alcaligenes faecalis* strain S-6. *J. Biochem.* **89**, 453-461.
4. Abraham, Z. H., Lowe, D. J. & Smith, B. E. (1993). Purification and characterization of the dissimilatory nitrite reductase from *Alcaligenes xylosoxidans* subsp. *xylosoxidans* (N.C.I.M.B. 11015): evidence for the presence of both type 1 and type 2 copper centres. *Biochem. J.* **295**, 587-593.
5. Masuko, M., Iwasaki, H., Sakurai, T., Suzuki, S. & Nakahara, A. (1984). Characterization of nitrite reductase from a denitrifier, *Alcaligenes* sp. NCIB 11015. A novel copper protein. *J. Biochem. (Tokyo),* **96**, 447-454.
6. Iwasaki, H. & Matsubara, T. (1972). A nitrite reductase from *Achromobacter cycloclastes*. *J. Biochem.* **71**, 645-652.
7. Zumft, W. G., Gotzmann, D. J. & Kroneck, P. M. (1987). Type 1, blue copper proteins constitute a respiratory nitrite-reducing system in *Pseudomonas aureofaciens*. *Eur. J. Biochem.* **168**, 301-307.
8. Inoue, T., Gotowda, M., Deligeer, Kataoka, K., Yamaguchi, K.,Suzuki, S. *et al*. (1998). Type 1 Cu structure of blue nitrite reductase from *Alcaligenes xylosoxidans* GIFU 1051 at 2.05 Å resolution: comparison of blue and green nitrite reductases. *J. Biochem. (Tokyo),* **124**, 876-879.
9. Godden, J. W., Turley, S., Teller, D. C., Adman, E. T., Liu, M. Y., Payne, W. J. & LeGall, J. (1991). The 2.3 Å X-ray structure of nitrite reductase from *Achromobacter cycloclastes*. *Science,* **253**, 438-442.
10. Kukimoto, M., Nishiyama, M., Murphy, M. E. P., Turley, S., Adman, E. T., Horinouchi, S. & Beppu, T. (1994). X-ray structure and site directed mutagenesis of a nitrite reductase from *Alcaligenes faecalis* S-6: roles of 2 copper atoms in nitrite reduction. *Biochemistry,* **33**, 5246-5252.
11. Dodd, F. E., Van Beeumen, J., Eady, R. R. & Hasnain, S. S. (1998). X-ray structure of a blue copper nitrite reductase in two crystal forms. The nature of the copper sites, mode of substrate binding and recognition by redox partner. *J. Mol. Biol.* **282**, 369-382.
12. Grossmann, J. G., Abraham, Z. H. L., Adman, E. T., Neu, M., Eady, R. R., Smith, B. E. & Hasnain, S. S. (1993). X-ray scattering using synchrotron radiation shows nitrite reductase from *Achromobacter xylosoxidans* to be a trimer in solution. *Biochemistry,* **32**, 7360-7366.
13. Grossmann, J. G. & Hasnain, S. S. (1997). X-ray scattering studies of metalloproteins in solution: a quantitative approach for studying molecular conformations. *J. Appl. Crystallog.* **30**, 770-775.
14. Strange, R. W., Murphy, L. M., Dodd, F. E., Abraham, Z. H. L., Eady, R. R., Smith, B. E. & Hasnain, S. S. (1999). Structural and kinetic evidence for an ordered mechanism of copper nitrite reductase. *J. Mol. Biol.* **287**, 1001-1009.
15. Prudêncio, M., Eady, R. R. & Sawers, G. (1999). The blue copper containing nitrite reductase from *Alcaligenes xylosoxidans*: cloning of the nirA gene and characterization of the recombinant enzyme. *J. Bacteriol.* **181**, 2323-2329.
16. Hall, J. F., Kanbi, L. D., Strange, R. W. & Hasnain, S. S. (1999). Role of the axial ligand in type 1 Cu centers studied by point mutations of met148 in rusticyanin. *Biochemistry,* **38**, 12675-12680.

17. Wittung-Stafshede, P., Hill, M. G., Gomez, E., Di Bilio, E., Karlsson, B. G., Leckner, J. *et al*. (1998). Title. *J. Biol. Inorg. Chem.* **3**, 367-370.
18. Gray, H. B. & Malmström, B. G. (1983). On the relationship between protein-forced ligand fields and the properties of blue-copper centers. *Comments Inorg. Chem.* **2**, 203-209.
19. Karlsson, B. G., Nordling, M., Pascher, T., Tsai, L. C., Sjolin, L. & Lundberg, L. G. (1991). Cassette mutagenesis of Met121 in azurin from *Pseudomonas aeruginosa*. *Protein Eng.* **4**, 343-349.
20. Murphy, M. E. P., Turley, S., Kukimoto, M., Nishiyama, M., Horinouchi, S., Sasaki, H. *et al*. (1995). Structure of *Alcaligenes faecalis* nitrite reductase and a copper site mutant, M150E, that contains zinc. *Biochemistry,* **34**, 12107-12117.
21. Boulanger, M. J., Kukimoto, M., Nishiyama, M., Horinouchi, S. & Murphy, M. E. P. (2000). Catalytic roles for two water bridged residues (Asp-98 and His-255) in the active site of copper-containing nitrite reductase. *J. Biol. Chem.* **275**, 23957-23964.
22. Kataoka, K., Furusawa, H., Takagi, K., Yamaguchi, K. & Suzuki, S. (2000). Functional analysis of conserved aspartate and histidine residues located around the type 2 copper site of copper-containing nitrite reductase. *J. Biochem. (Tokyo),* **127**, 345-350.
23. Prudencio, M., Eady, R. R. & Sawers, G. (2001). Catalytic and spectroscopic analysis of blue copper-containing nitrite reductase mutants altered in the environment of the type 2 copper centre: implications for substrate interaction. *Biochem. J.* **353**, 259-266.
24. Strange, R. W., Dodd, F. E., Abraham, Z. H. L., Grossmann, J. G., Brüser, T., Eady, R. R. *et al*. (1995). The substrate binding site in Cu nitrite reductase and its similarity to Zn carbonic anhydrase. *Nature Struct. Biol.* **2**, 287-292.
25. Murphy, L. M., Strange, R. W. & Hasnain, S. S. (1997). A critical assessment of the evidence from XAFS and crystallographic for the breakage of the imidazolate bridge during catalysis in CuZn superoxide dismutase. *Structure,* **5**, 371-379.
26. Olesen, K., Veselov, A., Zhao, Y., Wang, Y., Danner, B., Scholes, C. P. & Shapleigh, J. P. (1998). Spectroscopic, kinetic, and electrochemical characterization of heterologously expressed wild-type and mutant forms of copper-containing nitrite reductase from *Rhodobacter sphaeroides* 2.4.3. *Biochemistry,* **37**, 6086-6094.
27. Pascher, T., Bergstrom, J., Malmström, B. G., Vänngård, T. & Lundberg, L. G. (1989). Modification of the electron transfer sites of *Pseudomonas aeruginosa* azurin by site directed mutagenesis. *FEBS Letters,* **258**, 266-268.
28. Pascher, T., Karlsson, B. G., Nordling, M., Malmström, B. G. & Vänngård, T. (1993). Reduction potentials and their pH dependence in site-directed mutant forms of azurin from *Pseudomonas aeruginosa*. *Eur. J. Biochem.* **212**, 289-296.
29. Tsai, L. C., Bonander, N., Harata, K., Karlsson, G., Vanngard, T., Langer, V. & Sjolin, L. (1996). Mutant Met121Ala of *Pseudomonas aeruginosa* azurin and its azide derivative - crystal structures and spectral properties. *Acta Crystallog. sect. D,* **52**, 950-958.
30. Tsai, L. C., Langer, V., Sjölin, L. & Pascher, T. (1992). Crystallisation and preliminary crystallographic data for the azurin mutant Ala114 from *Pseudomonas aeruginosa*. *Acta Crystallog. sect. B,* **48**, 107-109.
31. Dodd, F. E., Hasnain, S. S., Abraham, Z. H. L., Eady, R. R. & Smith, B. E. (1997). Structures of a blue copper nitrite reductase and its substrate bound complex. *Acta Crystallog. sect. D,* **53**, 406-418.
32. Yanisch-Perron, C., Vieira, J. & Messing, J. (1985). Improved M13 phage cloning vectors and host strains: nucleotide sequences of the M13mp18 and pUC19 vectors. *Gene,* **33**, 103-119.
33. Studier, F. W. & Moffatt, B. A. (1986). Use of bacteriophage T7 RNA polymerase to direct selective high-level expression of cloned genes. *J. Mol. Biol.* **189**, 113-130.
34. Bolivar, F., Rodriguez, R. L., Greene, P. J., Betlach, M. C., Heyneker, H. L. & Boyer, H. W. (1977). Cloning and characterization of new cloning vehicles. II. A multipurpose cloning system. *Gene,* **2**, 95-113.
35. Sanger, F., Nicklen, S. & Coulson, A. R. (1977). DNA sequencing with chain-terminating inhibitors. *Proc. Natl Acad. Sci. USA,* **74**, 5463-5467.
36. Åasa, R. & Vänngård, T. (1975). EPR signal intensity and powder shapes a reexamination. *J. Magn. Reson.* **19**, 308-315.
37. MacGregor, C. H. (1978). Isolation and characterization of nitrate reductase from *Escherichia coli*. *Methods Enzymol.* **53**, 347-355.
38. Laemmli, U. K. (1970). Cleavage of structural proteins during the assembly of the haed of bacteriophage T4. *Nature,* **227**, 680-685.
39. Lowry, O. H., Rosebrough, N. J., Farr, A. L. & Randall, R. J. (1951). Protein measurement with the Folin phenol reagent. *J. Biol. Chem.* **193**, 265-275.
40. Leslie, A. G. W. (1992). Recent changes to the MOSFLM package for processing film and image plate data. *Joint CCP4+ESF-EAMCB Newsletter Protein Crystallog.* **26**, 000-.
41. CCP4, (1994). The CCP4 suite: programs for protein crystallography. *Acta Crystallog. sect. D,* **50**, 760-763.
42. Ramachandran, G. N., Ramakrishnan, C. & Sasisekharan, V. (1963). Title. *J. Mol. Biol.* **7**, 955.
43. Otwinowski, Z. & Minor, W. (1997). Processing of X-ray diffraction data collected in oscillation mode. In *Methods in Enzymology: Macromolecular Crystallography, part A* (Carter, C. W. J. & Sweet, R. M., eds), vol. 276, pp. 307-326, Academic Press.
44. Kraulis, P. J. (1991). MOLSCRIPT: a program to produce both detailed and schematic plots of protein structures. *J. Appl. Crystallog.* **24**, 946-950.
45. Merritt, E. A. & Bacon, D. J. (1997). Raster3D: photorealistic molecular graphics. *Methods Enzymol.* **277**, 505-524.
46. Esnouf, R. M. (1997). An extensively modified version of MolScript that includes greatly enhanced coloring capabilities. *J. Mol. Graph. Model,* **15**, 112-134.

Edited by R. Huber

(Received 21 August 2001; received in revised form 20 November 2001; accepted 26 November 2001)